Carbon on Platinum Substrates: From Carbidic to Graphitic Phases on the (111) Surface and on Nanoparticles†

Francesc Viñes,‡ Konstantin M. Neyman,§,|| and Andreas Görling*,‡

Friedrich-Alexander-Universität Erlangen-Nürnberg, Lehrstuhl für Theoretische Chemie and Interdisciplinary Center for Interface Controlled Processes, Egerlandstr. 3, D-91058 Erlangen, Germany, Departament de Química Física and Institut de Química Teòrica i Computacional (IQTCUB), Universitat de Barcelona, C/Martí i Franquès 1, 08028 Barcelona, Spain, and Institució Catalana de Recerca i Estudis Avançats (ICREA), 08010 Barcelona, Spain

Received: April 21, 2009; Revised Manuscript Received: July 24, 2009

The formation of carbonaceous deposits on Pt(111) surfaces and Pt nanoparticles has been studied using suitable models and density-functional calculations. The study addresses a broad range of processes, from the very first stage of carbon deposition up to a final building of graphene monolayers (ML) defined as a 1:1 ratio of the number of C atoms to surface Pt atoms. A carbidic phase is formed below a coverage of ∼0.3 ML, when negatively charged carbon atoms are strongly adsorbed preferentially on *fcc* hollow sites. On Pt nanoparticles, the adsorption of carbon atoms seems to be enhanced near particle edges due to the special flexibility of defect sites. Above a coverage of ∼0.3 ML, the formation of small C_n aggregates becomes possible. Interestingly, thermodynamics favors the formation of C_3 trimers at a coverage of 0.33 ML, whereas the formation of C_2 dimers requires a higher coverage of 0.5 ML. The covalently bonded C_2 species is supposed to be the key fragment for the formation of benzene-like rings at coverages above 0.6 ML. These rings are expected to be the building blocks for the graphene monolayer. However, the typical electronic structure of graphene is not observed until a coverage above ∼1.8 ML is reached. We corroborated the experimentally suggested carbon double-layer to be stable. It is proposed to consist of a monolayer of carbidic atoms C adsorbed on Pt with a graphene layer adsorbed on the carbidic layer. Some of the carbidic atoms serve as anchors for the graphene layer, with noticeably strong covalent bonds formed. This double-layer model would imply a much higher adhesion of the graphene layer than in the single-layer model.

1. Introduction

The interaction of carbon with transition metal (TM) surfaces and nanoparticles has been a subject of interest in the last decades for many reasons. An important motivation was that carbon is one of the major poisons of late TM (Pt, Ni, Rh, Ir, Pd, etc.) catalysts[1−3] commonly used for a broad range of reactions dealing with organic molecules, such as steam and dry reforming, partial oxidation, and others.[4] *De facto*, the carbon deposits are usually formed from dehydrogenation of hydrocarbons under reaction conditions.[5−8] They can aggregate on active sites of the catalysts, spoiling or modifying their reactivity by site-blocking and related effects. Thus, a careful investigation of the driving forces and mechanisms involved in the formation of such aggregates is urgently needed not only for deepening the academic knowledge but also for developing practical measures of making TM catalysts more resistant against reactivity modification and poisoning by carbon. This is the first goal of the present work.

Platinum, on which we focus in this work, proved to be a good catalyst in addition to the above-mentioned reactions for the reactions of water-gas shift,[9−12] CH_4 reforming by CO_2[13,14] (in the form of particles supported on reducible or acid oxides), hydrocarbon decomposition and dehydrogenation,[1,2,15−17] methanation,[18] and CO oxidation on Pt surfaces (of practical importance for the environmental pollution control).[19−28] Formation of carbon deposits that usually reduce the catalyst activity has been extensively studied in the decomposition of ethylene,[7,15,16,29,30] methane[31] (using supersonic molecular beams), and benzene[18] by means of low-energy electron diffraction (LEED)[5,7,8,18,32−34] and scanning tunneling microscopy (STM) experiments;[15,16,18,29,35−41] to a lesser extent, high-resolution electron-energy-loss spectroscopy (HREELS)[33,34] and Auger electron spectroscopy (AES)[6,8,18] have been applied. Many of these experiments indicate the formation of a graphitic overlayer, known as monolayer graphite (MG) or graphene,[7,8,15−18,31,33,37,38,42] merely being a single layer of the highly oriented pyrolitic graphite (HOPG) and sometimes also named so. These MG systems are of interest due to their proposed applications as stable field-electron emissors with an extremely inert surface.[43] Moreover, they can be attractive in the area of microelectronic devices, because of the spatially abrupt change of the electronic structure at the interface.[44] Unique electronic properties of graphene make it a highly promising advanced material also for other applications. Investigation of the formation of graphene on transition metal surfaces therefore is of interest and represents a second goal of this study.

On the Pt(111) surface, the MG graphene sheets expose the (0001) basal plane perpendicular to the support. Ethylene, the most common source of carbon for the formation of such layers, starts to decompose on the Pt(111) surface above 400 K,[45] and the partially negatively charged surface carbonaceous C_n^- species (called carbidic carbon)[1,2,45−47] can be detected at temperatures above 460 K.[48] Only after heating above 700 K

† Part of the "Walter Thiel Festschrift".
‡ Friedrich-Alexander-Universität Erlangen-Nürnberg.
§ Universitat de Barcelona.
|| Institució Catalana de Recerca i Estudis Avançats (ICREA).

10.1021/jp903653z CCC: $40.75
Published on Web 09/08/2009

(or 890 K using methane[31]), the typical ring-shaped LEED pattern of graphene emerges.[15] Initially, it was assumed that only one monolayer (ML) of graphite can be formed, because the Pt(111) surface catalyzes the ethylene decomposition, and cannot decompose ethylene once it is covered by a graphene layer.[15,16,37] However, recently, a procedure to obtain several layers of graphite on Pt(111) supports has been proposed.[29,49] The issues of how graphene is attached to the Pt(111) surface and of the differences with respect to a graphene layer on Ni(111) are a matter of discussion. Aizawa et al.[33] reported an in-plane C−C bond softening of MG adsorbed on Ni(111), due to an electron transfer from the substrate to the graphene π^* band,[33] in line with a modest interaction with the Ni(111) surface recently estimated in a density-functional (DF) study to be 42 kJ mol^{-1}.[50] No C−C bond softening is observed on Pt(111), indicating a weak adsorption. This lack of softening is similar to the situation found for graphene on transition metal carbide (TMC) (001) surfaces, illustrating the known parallelism of surface activity between TMC and Pt-group metals.[51−53] Moreover, the distance from the MG to the Pt(111) surface is distinctly large, 370 pm[8] (indicating a very weak adsorption interaction), compared to the distance between 280[30] and 310 pm[54] on Ni(111). Note that graphene layers are separated by 337 pm in bulk graphite.[42]

In fact, the hitherto only in the field theoretical study based on a DF method shows no adhesion at all of a commensurate graphene layer to the Pt(111) surface,[55] probably due to the lack of a description of van der Waals interactions by DF functionals. Nevertheless, to explain the long distance from MG to Pt(111) and the experimentally observed attachment, a double-layer model has been proposed by Zi-pu et al.,[8] where the first layer of carbon is located at 125 pm over the Pt(111) surface, forming a carbidic phase, while a MG is attached to this carbidic phase, at a distance of 245 pm, forming the so-called graphitic phase. This would imply a much stronger adhesion of the MG. The double-layer model could be an explanation for the small double-layer aggregates of up to 34 ± 7 carbon atoms detected by Land et al. at 500 K,[15] with the first carbon layer at a mean distance of 220 pm above the Pt(111) surface and the second one 210 pm above the first. Heating the sample to 773 K produced single-layer carbon particles located in average 230 pm above the metal surface.

Weak interaction of MG with the Pt(111) surface might be the origin of the broad variety of MG arrangements with respect to Pt(111) observed in LEED and STM experiments.[7,18,31,37] Moreover, there is a 13% mismatch of the graphene sheet lattice constant (246 pm) with respect to the lattice constant of Pt(111) [$a_o/(2\sqrt{2}) = 278$ pm]. Thus, the MG will adsorb incommensurate and exhibit moiré structures,[15,31,37,38] in contrast to Ni(111), where a commensurate MG is formed with a (1×1) LEED pattern.[30,50,54] On Pt(111), the most common moiré structure is present with a periodicity of 2.2 nm.[15,29,37] It is noteworthy that on STM images of graphite only half of the carbon atoms are bright,[56−58] which is usually explained in terms of the inequivalency of the carbon atoms in the uppermost graphite layer caused by the graphite layer atoms directly underneath.[59−62] However, the same STM behavior observed for Pt(111)-supported MG was assigned to the electronic structure particularities within the sheet.[15]

Many of the conclusions derived from the above-mentioned experiments remain tentative or partial without a theoretical corroboration. The present work is a state-of-the-art DF study providing theoretical insight into the formation of carbonaceous species on the (111) surface and nanoparticles of platinum from very low to high C coverage. To the best of our knowledge, this is the first theoretical study dealing with the formation of carbonaceous species from the isolated carbon atoms up to graphene sheets adsorbed on Pt surfaces.

TABLE 1: Calculated with Different *xc* Functionals and Experimental (exper.) Bond Lengths (*d*, pm) and Cohesive Energies (E_{coh}, kJ mol^{-1}) of Bulk Platinum and Bulk Graphite [*d*(C−C) Designates the Intralayer C−C Distances in Graphite]

	Pt bulk		graphite bulk	
source	*d*(Pt−Pt)	E_{coh}	*d*(C−C)	E_{coh}
VWN	276	696	244	860
PW91	282	558	247	766
PBE	281	559	245	757
RPBE	282	498	247	723
exper.	278[a]	563[b]	246[c]	711[d]

[a] Reference 8. [b] Reference 70. [c] Reference 42. [d] Reference 71.

2. Computational Details and Models

We performed DF calculations using the VASP code,[63] an implementation of a periodic plane-wave variant of the Kohn−Sham method. Interactions of valence electrons with the atomic cores were described by the projector augmented plane-wave method.[64] A kinetic energy cutoff of 415 eV for the plane-wave basis set was employed throughout, ensuring convergence of binding energies to better than 0.01 kJ mol^{-1}. Geometry optimizations were performed using a conjugate gradient algorithm until forces acting on each atom became less than 0.3 eV/nm. To speed up convergence of the Kohn−Sham self-consistent process, a Gaussian smearing of 0.2 eV has been applied, but the final energy values were extrapolated to 0 K (no smearing). Performed tests did not reveal any noticeable spin-polarization effect for either the substrate Pt models or the adsorption of carbon atoms on them. Thus, all calculations (except that of the free C atom) were non-spin polarized.

The search for transition states (TS) has been carried out in a point-wise fashion along the path connecting different adsorption configurations. The structures near the TS have been refined by a quasi-Newton method until forces are less than 0.3 eV/nm. The proper character of the adsorption minima and TSs has been confirmed by analysis of vibrational frequencies of the C atom through evaluation and diagonalization of the Hessian matrix, showing none (minimum) or only one (TS) imaginary vibrational frequency.

The lack of a universal exchange-correlation (*xc*) functional sufficiently accurately representing various observables of heavy-element systems[65,66] prompted us to examine several *xc* approximations in order to find out which of them provides most accurate adsorption energies and interatomic distances. The *xc* functionals employed were either within the local density approximation (LDA) [by Vosko−Wilk−Nusair[67] (VWN)] or the generalized gradient approximation (GGA) [by Perdew−Wang[68] (PW91), Perdew−Burke−Ernzerhof[69] (PBE), and the revised form of PBE[70] (RPBE)]. For benchmarking, we optimized Pt and graphite bulk materials. A Monkhorst *k*-point grid of $13 \times 13 \times 13$ was used for the Pt bulk optimization, while a $11 \times 11 \times 11$ *k*-points grid was used to compute graphite. In both cases, additional test calculations were done using different *k*-point meshes, ensuring that calculations with the above-mentioned meshes had a variation below 1 kJ mol^{-1} due to the *k*-points. Table 1 shows the bond distances and cohesive energies of the experimental and optimized bulk structures.[71,72] As

expected, LDA underestimates the bond distances in Pt by 2 pm and overestimates the bonding energy, due to the well-known overestimation of atomic interactions. GGA *xc* functionals provide better interaction energies, although the Pt−Pt bond lengths are overestimated by 3−4 pm. For graphite, RPBE yields results essentially matching the experimental values for the intralayer bond distances. As expected with none of the GGA *xc* functionals, the interlayer bond distance could be obtained correctly because van der Waals interactions, which are crucial for the interlayer bonding, are not taken into account by GGA *xc* functionals. Much too large interlayer distances or no bonding at all was found for the tested GGA functionals. Since none of the *xc* functionals clearly performs better, and keeping in mind that the present study focuses on interaction energies rather than on bond distances, the RPBE functional proven to give better adsorption energies[70] has been chosen as a default in all calculations, unless stated otherwise. The LDA *xc* functional has been occasionally used when weak interactions were present. In such a way, one could expect some compensation by overestimated bonding of the lacking description of dispersive forces—van der Waals interactions are not accounted for—by the contemporary *xc* functionals; as we show below, this can be important for MG on Pt(111).

We define the calculated adsorption energy E_{ads} of a carbon atom on a Pt substrate as

$$E_{ads} = -E_{C/Pt} + (E_C + E_{Pt}) \quad (1)$$

where $E_{C/Pt}$ is the total energy of the adsorption system, E_C the energy of the isolated atom C, and E_{Pt} the total energy of the relaxed Pt substrate, either Pt(111) surface or Pt_n nanoparticle. According to this definition, positive energy values correspond to favorable adsorption. When more than one C atom is adsorbed on the substrate (per unit cell), E_{ads} as well as other energies (see below) are given per carbon atom. The isolated atomic C reference has been calculated in the middle of a broken-symmetry unit cell of dimensions $9 \times 10 \times 11$ Å. For situations with more than one C per unit cell or Pt_n nanoparticles, we additionally define an interaction energy, E^{int}_{PtC}, of carbon layers or more generally carbon structures with the Pt substrate as

$$E^{int}_{PtC} = -E_{C/Pt} + (E_{Car} + E_{Pt}) \quad (2)$$

where E_{Car} is the energy of the C subsystem calculated at the adsorbed geometry but without substrate. E_{Car} results from a single-point calculation with the same parameters as those used for the complete adsorption system, and this allows one to estimate two contributions to the adsorption energy: (i) the interaction with the substrate and (ii) the interaction between adsorbates. The difference between E_{int} and E_{ads} provides the interaction energy between the carbon atoms adsorbed on the surface, which we name E^{int}_{CC}

$$E_{ads} = E^{int}_{PtC} + E^{int}_{CC} \quad (3)$$

The reference Pt(111) surface model is a six-layer slab. Positions of atoms in the bottom three layers were kept frozen as optimized for Pt bulk, whereas the other three layers (closer to adsorbates) were allowed to relax completely. An intralayer vacuum space of 1 nm thickness was introduced to avoid interactions between repeated slabs. Figure 1 shows the employed Γ-centered *k*-point grids together with the surface unit cells employed in this study. The *k*-point grids are dense enough to guarantee a convergence with *k*-points of at least 1 kJ mol^{-1}, as revealed by test calculations. Because of the large vacuum space, only one *k*-point is needed in the vacuum direction of the slab cell.

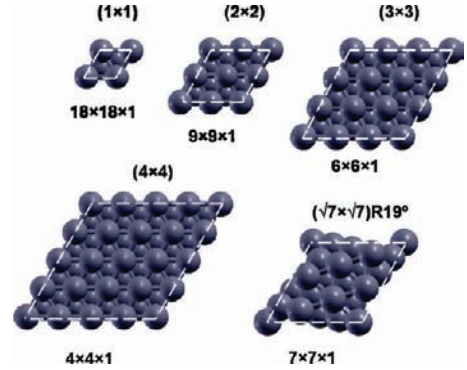

Figure 1. Surface unit cells of Pt(111) slabs (with the borders indicated by dashed lines) employed throughout the study. The *k*-point grids employed are displayed for each surface unit cell.

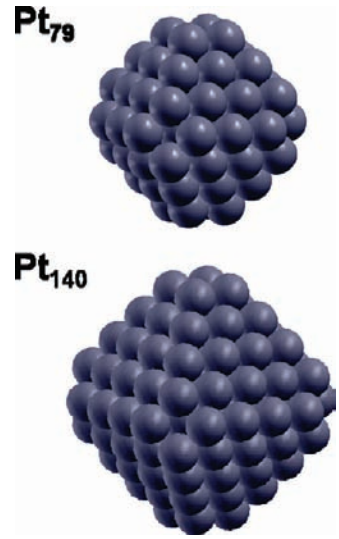

Figure 2. Studied cuboctahedral Pt_{79} and Pt_{140} model nanoparticles exposing small (100) and larger (111) facets.

Cuboctahedral metal nanoparticles of already ∼80 atoms have been proven to provide essentially size-converged results for the adsorption properties (including energies) of species on them[73] and to be representative of the interaction between much larger nanoparticles.[74] Moreover, such properties as average cohesion energy and average metal−metal bond distance reveal scalability with respect to size up to the bulk limit.[66,75] These nanoparticles can ideally complement the slab models, enabling the study of interactions with defect sites (at edges, corners, etc.), present in significant number on supported metal catalysts and often responsible for their special catalytic activity. Such a combined modeling strategy has been applied successfully in the past.[76,77] Here, we used two cuboctahedral Pt nanoparticles depicted in Figure 2, Pt_{79} and Pt_{140}, to obtain microscopic information about the interaction of carbon with defects on model Pt catalysts. One such nanoparticle was placed in the middle of a large cubic unit cell, leaving 1 nm of vacuum in each direction of the unit cell in order to avoid interactions between the images in adjacent unit cells. All calculations on Pt_n nanoparticles were performed at the Γ-point, i.e., using one *k*-point.

TABLE 2: Adsorption Energies, E_{ads} (kJ mol^{-1}), of a Single C Atom at Different Surface Sites of Pt(111) as Obtained in RPBE Slab Calculations with Different Surface Unit Cells and Carbon Coverages, θ_C: on Top of a Surface Pt Atom (top), Bridging Two Surface Pt Atoms (bridge), at an *fcc* or *hcp* Three-Fold Hollow Site

surface unit cell	θ_C, ML	*fcc*	*hcp*	bridge	top
(2 × 2)	$^1/_4$	653	637	566	425
(3 × 3)	$^1/_9$	659	645	576	440
(4 × 4)	$^1/_{16}$	647	633	564	436

TABLE 3: Diffusion Barriers (kJ mol^{-1}) of Single Carbon Atoms between *fcc* and *hcp* Sites at Decreasing Coverage (Estimated Diffusion Temperature, T_{diff}, in K)

θ_C, ML	*fcc* → *hcp*	*hcp* → *fcc*	T_{diff}
$^1/_4$	87	71	486
$^1/_9$	83	69	464
$^1/_{16}$	83	69	464

3. Results and Discussion

3.1. Adsorption of Carbon Atoms. First, the adsorption of C atoms in a low-coverage regime has been considered. We define carbon coverage θ_C as the ratio of the number of deposited C atoms n_C to the number of surface (upper layer) Pt atoms n_{Pt} per unit cell

$$\theta_C = n_C/n_{Pt} \quad (4)$$

Thus, one layer that contains more atoms than the surface Pt atoms is characterized by $\theta_C > 1$ ML. Below, we address overlayers up to $\theta_C = 2^2/_3$ ML.

Table 2 shows the E_{ads} values for the adsorption of a single C on different unit cells equivalent to a coverage θ_C from $^1/_{16}$ to $^1/_4$ ML. For all coverages under scrutiny, 3-fold hollow face-centered-cubic (*fcc*) and hexagonal-cubic-packed (*hcp*) surface sites are definitely preferred over the lower-coordination bridge and top sites. There is no clear trend in the coverage dependence of the adsorption energies that vary with θ_C by at most 15 kJ mol^{-1} (an effect of the repulsion between negatively charge C atoms appears at higher coverage, as will be shown below). At each θ_C, C on the *fcc* site is 14−16 kJ mol^{-1} more stable than on the *hcp* site. The origin of this slight yet noticeable difference can be a steric repulsion between the electron density of the adsorbate C and the atom Pt of the second substrate layer located directly under an *hcp* site. This effect was not observed previously on Pd, and might be the shorter metal−metal distance of Pd, which would lead to a screening of the electron density of the inner layers.[77] The present results are in line with experimental values of 627−628 kJ mol^{-1},[1,17,78,79] and comparable with previous DF data of Michaelides et al. (~680 kJ mol^{-1})[80] and Kua et al. (636 kJ mol^{-1}).[81] However, the present results show preferred occupancy of *fcc* sites, instead of *hcp* sites, which was obtained by Michaelides et al.[80] using the PW91 *xc* functional and a three-layer slab in the geometry kept fixed as in Pt bulk. The results of Kua et al.[81] obtained with the B3LYP *xc* functional do not distinguish between *fcc* and *hcp* sites, since they calculated a one-layer Pt_8 cluster (at experimental Pt−Pt distances). We examined the possible effect of the lower-lying Pt layers by adsorbing C on the (3 × 3) surface slab unit cell and letting four of the outermost layers relax instead of the three outermost layers, thus fixing Pt atomic positions in only two instead of three layers representing the Pt bulk; only a slight E_{ads} decrease of 2 kJ mol^{-1} is found. In this sense, the present substrate relaxation approach seems to be appropriate, and to the best of our knowledge, we communicate here DF results for the so far most accurate models of carbon adsorption on a Pt(111) surface.

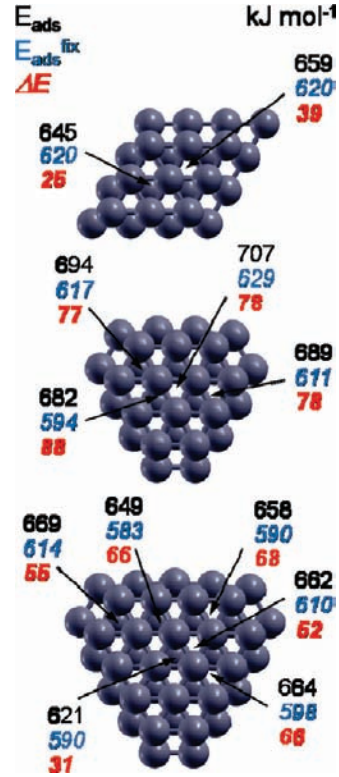

Figure 3. Adsorption energies of carbon on a Pt(111) (3 × 3) slab (top panel) and on Pt_{79} (middle panel) and Pt_{140} (bottom panel) nanoparticles. Only two layers are shown, to enable a simple distinction between *fcc* (without an atom in the second layer) and *hcp* sites (with an atom in the second layer). Adsorption energies obtained with a frozen substrate (E_{ads}^{fix}) and differences with respect to E_{ads} (ΔE) are also displayed.

On the other hand, adsorption on top of a surface Pt atom and at a position bridging two Pt atoms turned out to be TS according to a frequency analysis always showing one imaginary frequency. Thus, bridge sites between *fcc* and *hcp* sites can be considered as TS for carbon diffusion on the surface. An examination of the diffusion energy barriers in Table 3 reveals that in the considered coverage range the diffusion barrier barely changes, by 4 kJ mol^{-1} or less, i.e., below the chemical accuracy. Our estimates of the diffusion temperature (see Table 3) following the procedure described elsewhere[82,83] give the values in line with 460 K needed to detect C_n^- species.[48]

The adsorption of C was investigated also on the Pt_{79} particle. Figure 3 (middle panel) shows E_{ads} values on all possible 3-fold hollow sites. The adsorption energy of a C atom on a small four-atomic (100) facet of Pt_{79} is 671 kJ mol^{-1}. In contrast to Pd_n nanoparticles,[77] a single C on platinum 3-fold hollow sites is thermodynamically more stable than on the 4-fold hollow sites of (100) facets, by at least 10 kJ mol^{-1}. Interestingly, there is a clear increase of the C adsorption energy on (111) facets, of 30−50 kJ mol^{-1}, as compared with $^1/_9$ coverage adsorption on the Pt(111) slab (Figure 3, top panel). The *fcc* central site exhibits the largest adsorption energy increase, with $E_{ads} = 707$ kJ mol^{-1}. This finding is different from the anticipated adsorption energy enhancement in the vicinity of such low-coordinated sites as edges/corners. The reason could be that (111) facets of Pt_{79} are still somewhat too small for providing a quantitatively

representative description of such strong adsorption interaction with an extended Pt(111) surface as that of C. In fact, comparison with adsorption energy values obtained using a frozen substrate (named E_{ads}^{fix}) results in ~80−90 kJ mol^{-1} contributions to the adsorption energy due to the relaxation of the Pt_{79} particle. This is more than 10% of the adsorption energy E_{ads} and reveals the importance of the structural adjustment of substrate for C accommodation. On a Pt(111) surface, on the other hand, this contribution is smaller, of ~25−40 kJ mol^{-1}. Interestingly, the latter indicates that substrate relaxation may be a reason for the slightly different activity of *fcc* and *hcp* sites. In fact, substrate relaxation agrees with a partial steric repulsion between C and *hcp* sites. On both *fcc* and *hcp* sites, surface Pt atoms move outward by 13 and 15 pm, respectively, induced by the presence of C. Additionally, the Pt−Pt bond lengths of the 3-fold hollow sites increase by 25 and 17 pm for the *fcc* and *hcp* sites, respectively. However, the most meaningful difference is that when substrate is allowed to relax; C is placed at a 94 pm height above *hcp* sites and only 86 pm over *fcc* sites. The larger height over *hcp* sites agrees with a steric repulsion with the second-layer Pt atoms of *hcp* sites. To further address this point, the adsorption of C on 3-fold hollow sites was considered also on (111) facets of the Pt_{140} model (Figure 3, bottom panel). The adsorption energies on the latter are closer to the slab values; however, an enhancement of substrate relaxation is observable at edges/corners. Despite the fact that there is no significant stabilization of C on *fcc* sites, there is an extra stabilization on *hcp* sites at edges/corners, leading to an interaction strength competitive with that on *fcc* sites.

Another point of interest is the formation of subsurface C species, which have been demonstrated recently to strongly affect the catalytic activity of the Pt-group metals, Ni and Pd.[84−87] One of spectacular examples was enhanced activity of the partial hydrogenation of alkynes on Pd.[87] In fact, C atoms have been proven to be thermodynamically stabilized subsurface of both Ni(111)[50] and Pd(111)[77,88] single crystals as well as in PD nanoparticles,[77,89] if located in octahedral subsurface (*oss*) and even in tetrahedral subsurface (*tss*) sites between the top (surface) and the subsequent (subsurface) (111) metal layers. Such carbon phases can destabilize nearby surface species, like it has been shown for CO adsorption.[89,90] This destabilization can be at the origin of the activity and selectivity enhancement. In contrast with other studies,[91] our recent calculations[77] showed that C atoms sink subsurface at edge sites of Pd_n nanoparticles essentially *without a barrier*. It suggests that the C-induced modification of catalytic activity occurs at the most active (edge and corner) sites of model catalysts and it is possible at very low temperatures/coverages.

Because of the new interest in subsurface carbon species, we studied two models of carbon in the Pt subsurface. In one case, C atoms were placed in *oss* sites of Pt(111), at $\theta_C = {}^1/_9$ ML. In another case, a single C was in an *oss* site at the edge between (111) facets of Pt_{79}. These sites were chosen because they provide more space to accommodate C atoms; moreover, the edge flexibility of Pt_{79} can enhance the subsurface C stabilization. However, the calculations showed a carbon destabilization of 59 kJ mol^{-1} on Pt(111) and 53 kJ mol^{-1} on Pt_{79} compared to the adsorption on the corresponding *fcc* sites. Thus, on Pt, sinking atomic carbon into the substrate seems hardly possible, which is very different from the other two metals of the same group. Less stable single C on 4-fold hollows of (100) facet Pt_n moieties with respect to the lower-coordinated *fcc* and *hcp* sites on the (111) facets is at variance with preferential carbon stabilization in the sites with the highest available coordination, which is found for C/Pd systems. This feature could be considered as an indication of such a different thermodynamics with respect to the lacking subsurface stabilization of C on Pt.

TABLE 4: Adsorption Energy per Atom for the Adsorption of Two Carbon Atoms (Named C^1 and C^2) on a (2 × 2) Slab Model ($\theta_C = {}^1/_2$) (Site Occupation and the Shortest Distance between C Atoms, $d(C^1-C^2)$, Are Also Shown)

site C^1	site C^2	$d(C^1-C^2)$, pm	E_{ads}, kJ mol^{-1}
bridge	bridge	133	562
fcc	*hcp*	326	566
hcp	*hcp*	282	566
fcc	*fcc*	282	577
fcc	*hcp*	137	590

TABLE 5: Adsorption Energies per Carbon Atom for a C_2 Dimer Formed at Neighboring *fcc* and *hcp* Sites and Two Single C Atoms (at the Nearby *fcc* Sites) for Different θ_C (and Surface Unit Cells) [$d(C^1-C^2)$ Is the Nearest C−C Distance]

		dimer C_2		single C	
θ_C, ML	surface unit cell	E_{ads}, kJ mol^{-1}	$d(C^1-C^2)$, pm	E_{ads}, kJ mol^{-1}	$d(C^1-C^2)$, pm
${}^1/_8$	(4 × 4)	605	137	654	565
${}^2/_9$	(3 × 3)	607	137	651	489
${}^1/_3$	(3 × 3)	600	137	634	489
${}^1/_2$	(2 × 2)	590	137	577	282

3.2. Formation of C_n^- Species. In a second step, we investigated the formation of small surface C aggregates, addressing their experimental detection.[48] For that, the formation of C_2 dimers was studied as a function of C−C separation at $\theta_C = {}^1/_2$ ML. According to the results listed in Table 4, stable dimers are formed with one C atom on a *fcc* site and another on a neighboring *hcp* site. This system is 28 kJ mol^{-1} more stable than the found minimum where a dimer is formed having each of the two carbon atoms above neighboring surface bridge sites. Optimization of the C−C distance (together with the specific site occupation) seems to be the main driving force for the stabilization, but can dimers be formed at lower coverage? To this end, a comparison of dimers with two separate atoms was carried out at $\theta_C = {}^1/_8$, ${}^2/_9$, and ${}^1/_3$ ML. The results listed in Table 5 show that at these coverages the C_2 dimer remains less stable than two single adsorbed atoms. At a coverage of $\theta_C = {}^1/_2$ ML, the situation changes. At this point, the significant mutual repulsion of two negatively charged atomic C species and the formation of a covalent C−C bond between them turn out to be energetically competitive. The formation of C_2 dimers was also inspected on Pt_{79} nanoparticles. The most stable C_2 dimer found located near particle edges occupying *fcc* and *hcp* sites is 36 kJ mol^{-1} destabilized over the situation when two C atoms occupy the most stable (central *fcc*) sites of opposite facets. Thus, compared with the smallest coverage $\theta_C = {}^1/_8$ ML on Pt(111), it seems that the edge effect enhances somewhat the formation of the dimers. Nevertheless, C_2 dimers still remain energetically unfavorable compared to single C atoms at large distances. This indicates that even in the presence of such defect sites as nanoparticle edges the formation of C_2 dimers from single adsorbed C atoms on Pt requires achievement of a certain critical coverage value θ_C.

A C_2 dimer adsorbed on Pt(111) surface is depicted in Figure 4. The electron localization function (ELF) clearly shows a covalent bond between C atoms in the dimer. Moreover, density of states (DOS) plots (see Figure 5) also manifest the formation of covalent-like orbitals, with mixing of C_{2s} and C_{2p} states. The total Bader charge of the adsorbed dimer, −0.48 e, essentially

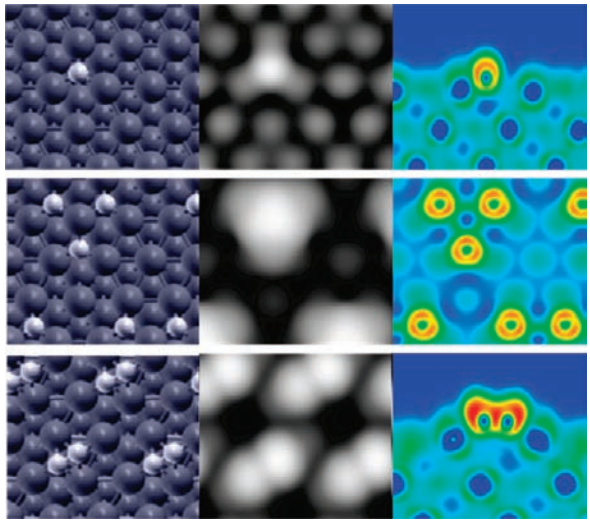

Figure 4. Image of the disperse C, C_3, and C_2 aggregate overlayers on Pt(111) (top, middle, and bottom images, respectively): (left column) top views; (middle column) calculated STM images; (right column) ELF images (side views for C and C_2, top view for C_3).

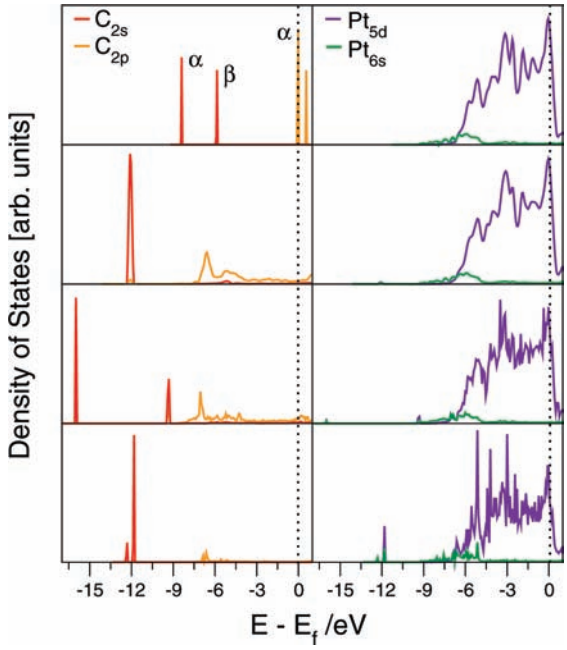

Figure 5. Density of states (DOS) plots for an isolated C atom (uppermost left panel), the clean Pt(111) surface (uppermost right panel), and below similar plots for the adsorption of single C atoms, C_2 dimers, and C_3 trimers, consecutively.

coincides with the charge of single adsorbed C atoms. Thus, the overall amount of charge on the adsorbates remains unchanged when going from single C atoms to C_2 dimers, and only a redistribution of the charge among the C atoms takes place. Calculated STM images taken at constant-current mode with intensity $I = 0.0001$ nA and voltage 0.1 eV (Figure 4) show the repeated arrangement.

The formation of C_3^- aggregates was investigated in a similar way. For this purpose, all of the possible arrangements of three C atoms on a (3×3) unit cell of the Pt(111) surface were optimized. This included situations with single disperse C atoms, each occupying either *fcc*, *hcp*, or a combination of these sites, C_3 clusters around surface Pt atoms, *fcc* or *hcp* hollows, as well as rows of atoms adsorbed on *fcc* and *hcp* hollows. The adsorption energies of the most stable arrangements under scrutiny are listed in Table 6. There are only small energy differences of ≤ 10 kJ mol^{-1} between these arrangements, while the rest of the cases studied (not included) presented adsorption energies which were at least 20 kJ mol^{-1} smaller than the most stable conformations found. Focusing on the most stable ones, it turns out to be that trimers seem to be slightly preferred over three single adsorbed C atoms. Thus, formation of trimers appears to be possible at a coverage of $^1/_3$ ML. Hence, the trimers are energetically more favorable than dimers, in the sense that the former can be built at lower coverage. In the most stable C_3 trimer, each of its three C atoms occupies an *fcc* site around one surface Pt atom. The Bader charge analysis shows again a charge of -0.46 e for the whole C_3 cluster, shared between the carbon atoms. The thermodynamically driven formation of trimers before dimers is a surprising result. However, it must be handled with caution, since kinetics can play a decisive role in such processes. In contrast with dimers, no clear C−C bond is formed in the trimers on Pt(111), as evidenced by the lack of a high ELF between C atoms (Figure 4); concomitantly, C−C distances in C_3, 310−313 pm, are too long to imply a notable covalent bonding. DOS plots show a more prominent mixing of C_{2p} states with Pt_{6s} and Pt_{5d} surface states than in the dimer case.

TABLE 6: Adsorption Energies per Carbon Atom for C_3 Trimers Formed around a Pt Atom on the (111) Surface with the Three C Atoms Occupying Neighboring *fcc* and *hcp* Sites and for Single C Atoms (Occupying *fcc* Sites) at a Coverage of $^1/_3$ ML [*d*(C−C) Is the Shortest C−C Distance between Two C Atoms]

adsorbate	sites	E_{ads}, kJ mol^{-1}	*d*(C−C), pm
trimerC_3	*fcc*	638	310
trimerC_3	*hcp*	630	313
single C	*fcc*	634	489
single C	*hcp*	628	489

An experimental identification of the formation of trimers could be proposed by high-resolution STM images, such as the calculated one displayed in Figure 4. Other experimental identifications of carbon trimers could come from measurements of the work function (ϕ). The latter is defined as the energy necessary to transfer one electron from the Fermi level (E_F) to the vacuum. Thus, an estimate of ϕ can be calculated as

$$\phi = V - E_F \tag{5}$$

where V is the potential energy of one electron in the vacuum. The Fermi energy level is given by the last occupied orbital, and the V term is estimated with the help of the potential energy distribution in the employed cell. The calculated values of ϕ for a situation of single C atoms ($\theta_C \leq {}^1/_4$ ML) oscillate between 5.52 and 5.47 eV. The work function for a dimer at $\theta_C = {}^1/_2$ ML is estimated to be 5.45 eV. In both cases, the dipole seems to insignificantly affect the work function because of the proximity of the carbon atoms to the Pt surface. However, for the trimer, the estimated work function value of 4.89 eV is distinctly different. This reduction of the work function can be partly assigned to the noticeable, of 182 pm, elevation toward the vacuum of the surface Pt atom, to which the C_3 moiety is bound and which becomes located even above the C_3 plane (see Figure 6). Indeed, this Pt atom carries a positive charge of 0.12 e and the corresponding dipole moment formation would act to reduce the work function. Similar results are found when having the C_3 moiety on the Pt_{79} nanoparticle.

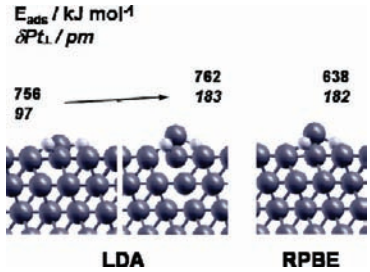

Figure 6. Side view of carbon trimers calculated at LDA and RPBE levels. Adsorption energies, E_{ads}, and the elevation of the central Pt atom toward the vacuum, $\delta Pt_\perp$, are listed.

In any case, such a very big displacement of the Pt atom out of the surface is interesting and could even lead to an enhanced activity of Pt, because of the lack of coordination of these shifted Pt atoms. However, it needed to be confirmed that this result is not an artifact of the RPBE *xc* functional used that underestimates the interatomic interactions and possibly makes surface Pt atoms too weakly bound and thus too easily removable. To this end, calculations with an interaction-overestimating LDA *xc* functional were performed. The results (Figure 6) show that the elevation is found again, although an intermediate local minimum with the Pt atom still below the C_3 plane is found. However, the final structure closer to the RPBE one is 6 kJ mol^{-1} thermodynamically more favorable. The intermediate local minimum found suggests that a small barrier must be present at the LDA level, although within the RPBE description the elevation of the Pt atom occurs *without a barrier*. Thus, even if present, the small barrier has to be overcome already at very low temperature. Finally, C_3 trimers with a C−C distance of 320 pm are found on Pt_{79} on the nanoparticle facets. The overall energy gain of the trimer with respect to a case of three single distant C atoms on Pt_{79} is 14 kJ mol^{-1}. Thus, the cluster model yields results similar to those that we have calculated for Pt(111).

The interplay of dimers and trimers has been studied at a coverage of $^4/_9$ ML. At this coverage, a situation where a trimer and an isolated carbon atom at a *fcc* site are present on the surface leads to an adsorption energy per atom of 612 kJ mol^{-1}, i.e., stabilized by 5 kJ mol^{-1} per atom with respect to two adsorbed dimers. At $\theta_C = {}^2/_3$ ML, dimers are clearly preferred to trimers, the former are characterized by an adsorption energy of 598 kJ mol^{-1} and the latter −533 kJ mol^{-1}. However, at this coverage, the formation of benzene-like rings starts to become thermodynamically preferred. Such ring formation implies that one-half of the C atoms adsorb on top of surface Pt atoms while the other half are adsorbed either in *fcc* (E_{ads} = 603 kJ mol^{-1}) or *hcp* (E_{ads} = 604 kJ mol^{-1}) positions. The formation of C_6 rings could be noticed in STM images (see Figure 7). It is worth pointing out that C_6 rings were not competitive structures at lower coverage. Also, note that, in a ring arrangement, the global charge transfer is bigger, with a Bader charge of −0.20 e for C atoms over *hcp* and *fcc* sites but of −0.88 e for those located on top of surface Pt atoms. Surprisingly, the resulting dipole causes almost no change in the work function, which in this case is computed to be 5.38 eV. In addition, the rings are not perfect (see Figure 7), with C−C distances of 142 pm and two different C−C−C angles (134 and 106°). Finally, the ELF images expose big charge globes between C atoms, and also in the direction where a H−C bond would be found in benzene. These benzene-like rings can act as a building block for the formation of graphene layers, as will be studied in the following.

3.3. Formation of Graphene. In this section, the formation of graphene or quasi-graphene layers on Pt(111) surfaces is considered. The benzene-like rings described in the last section are still the most stable conformation at a coverage of $1^1/_2$ ML, with an E_{ads} value of 611 kJ mol^{-1} (on-top/*fcc*) or 612 kJ mol^{-1} (on-top/*hcp*); see Table 7. At this coverage, distorted rings are still present, although the C−C distance reduces to 140 pm, and bond angles become 125 and 115°; thus, a graphene-like structure is approached. Moreover, the work function is reduced to 5.08 eV, again approaching the graphene value of about 4.8 eV.[92] The ELF pictures and STM images are similar to those of a coverage of $^2/_3$ ML discussed in the previous section. The partial occupation of either *hcp* or *fcc* sites by half of the carbon atoms in the benzene-like rings is accompanied by a small difference in the adsorption energy (of at most 1 kJ mol^{-1}) for the two possibilities. The situation changes drastically at a coverage of θ_C = 2 ML, when an occupation of both on-top and *fcc* sites provides an E_{ads} value of 634 kJ mol^{-1}, while only 539 kJ mol^{-1} corresponds to on-top/*hcp* sites. At this coverage, perfect rings are formed, and the saturation is reflected with high ELF globes between carbon atoms (Figure 7). The interaction of the carbon layer with the substrate is noticeable, since the carbon layer is located 229 pm above the Pt surface (see Figure 7). Moreover, the effect of the substrate is translated in a STM image where half of the C atoms are shown as bright points while the other half are marked as more shadow spots. The Bader charges show no charge transfer between the Pt(111) surface and the C layer.

In contrast, when the coverage is raised to $2^2/_3$ ML, the interaction with the substrate become so small that no difference in adsorption energy is observed by the occupation of *fcc*, *hcp*, on-top, or bridge sites. At this coverage, the adsorption energy of 726 kJ mol^{-1} approaches the computed graphene formation energy, which we estimated as 727 kJ mol^{-1}. In addition, the C−C distance is 141 pm and, thus, close to the experimental value of 143 pm. Thus, one can indeed talk about a graphene layer formed at a coverage of $2^2/_3$ ML. Moreover, the work function estimated to be 4.71 eV almost matches the computed work function of graphene, 4.73 eV. Here, it is noteworthy that RPBE predicts a graphene layer placed 430 pm above the Pt surface. The disagreement with the experimental value of 370 pm[8] may be caused by the compression of the graphene layer compression in the calculation to match the Pt substrate (the graphene layer is compressed by about 13%, corresponding to the mismatch with the Pt(111) lattice constant).[15,31,37,38] To shed light on this matter, a calculation for the smallest experimentally observed graphene overlayer was carried out, a $(\sqrt{7} \times \sqrt{7})$R19° periodicity of Pt(111) with a (3 × 3) unit cell of graphene.[37] However, the same results were obtained for the adsorption energy, while a longer distance of 479 pm between the graphene layer and the Pt surface was found. Thus, the compression seems to have little effect on the adsorption energy and the graphene−Pt distance. Another explanation could come from the fact that the RPBE *xc* does not take into account dispersive interacting forces, which may be important in this case. LDA calculations, which overestimate bonding, yield a too short distance of 318 pm between the graphene layer and the Pt surface (322 pm for the $(\sqrt{7} \times \sqrt{7})$R19° arrangement). Thus, not surprising, none of the present *xc* functionals is able to accurately describe the weak interactions between a single graphene layer and the Pt(111) surface. This lack of interaction would also explain the calculated STM image, where all of the C atoms are shown as bright points (see the bottom of Figure 7).

The evolution from C_6 groups to graphene is also traced in the PDOS (Figure 8). Here, diverse bands are observed at coverages of $^2/_3$ and $1^1/_2$ ML below −10 eV, showing the

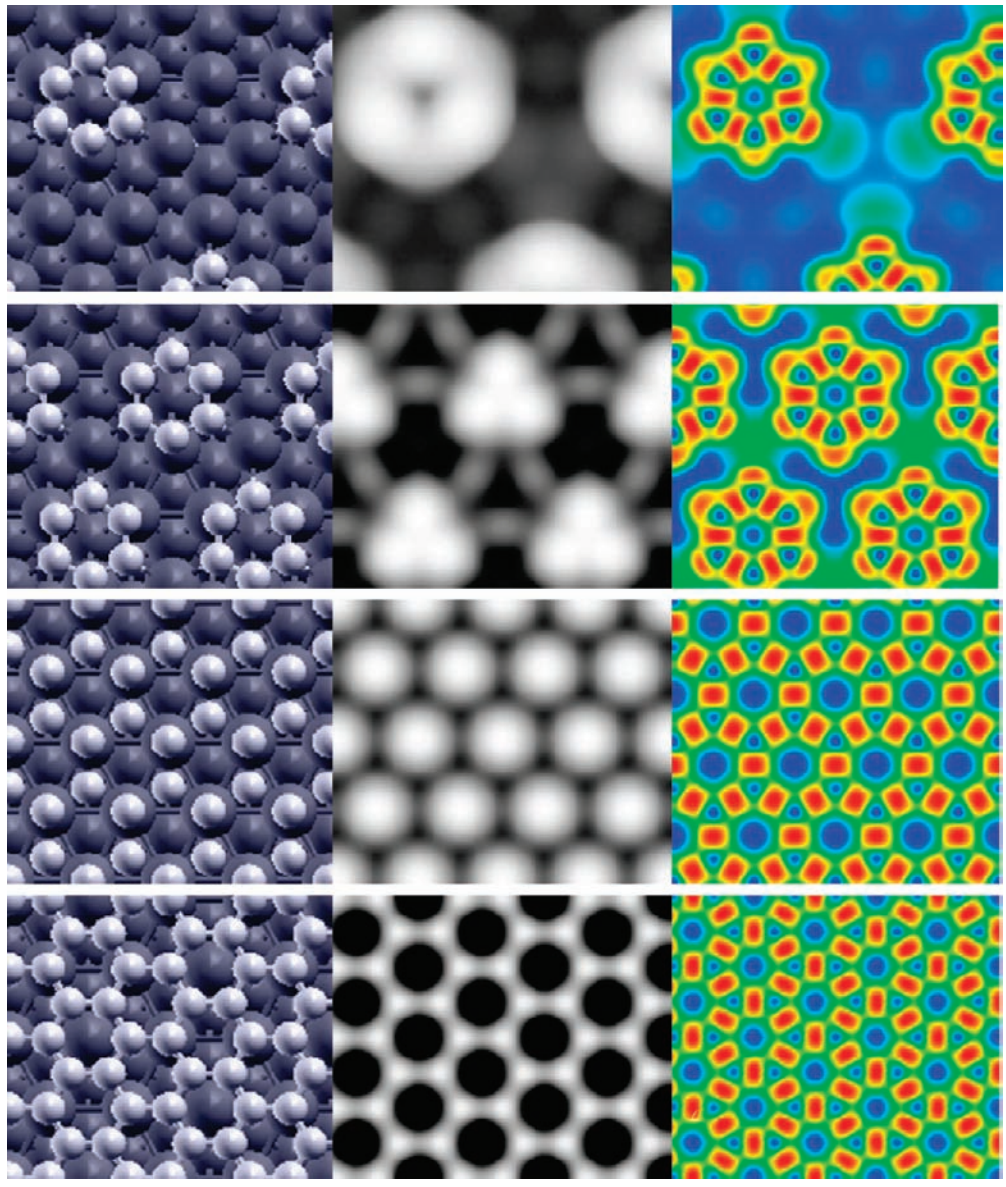

Figure 7. Calculated data (top views) for C_6 rings on Pt(111) at increasing coverages of $^2/_3$, $1^1/_2$, 2, and $2^2/_3$ ML (from top to bottom): (left column) structure sketch; (middle column) constant-current calculated STM images; (right column) ELF plots.

TABLE 7: Adsorption Energy E_{ads} per C Atom Caclulated for the Benzene-Like Rings on the Pt(111) Surface at Increasing Carbon Coverage θ_C (C Atoms of the Rings Occupy Top and *fcc* Sites)

θ_C	E_{ads}, kJ mol^{-1}
$^2/_3$	603
$1^1/_2$	611
2	634
$2^2/_3$	726

increasing formation of covalent bonds, mixing s and p orbitals. At a coverage of 2 ML, the mixing of C orbitals with Pt states starts to vanish, while graphene-like structures emerge.

At this point, the possible existence of the double-layer model was also investigated. Many arrangements were tested, for a coverage of $3^2/_3$ ML, similar to the C/Pt ratio reported by Zi-pu et al.[8] The most stable conformation (see Figure 9) implies that a first layer of carbon with a coverage of 1 ML is formed, occupying *fcc* sites. Over this layer a graphene layer is formed in such a way that some of the graphene C atoms are located directly on top of the carbon atoms of the first layer (another carbon atom of the graphene layer is located above $^2/_3$ ML of the carbidic carbon atoms). In fact, there are covalent bonds not only between carbon atoms of the graphene layer but also between carbon atoms of the carbidic and graphitic layers. Such covalent bonds serve as anchor points for the graphene layer. In fact, the calculated interaction energy between the carbidic and graphitic layers is 169 kJ mol^{-1} per anchor C atom. The interaction energy of the carbon atoms of the carbidic layer to the Pt surface is 381 kJ mol^{-1}, thus much smaller than that of isolated C atoms at low coverage. The results show a downward displacement of some of the graphitic atoms, and the upward movement of some of the carbidic atoms. Thus, the carbidic as well as the graphene layer could be considered to be split into two sublayers. One of the carbidic sublayers having $^1/_3$ of the atoms located 66 pm above the Pt(111) surface, the other having $^2/_3$ of the atoms located at 126 pm. The graphene sublayers have $^1/_3$ of the carbon atoms at 283 pm and $^2/_3$ at 326 pm. Although our calculations corroborate the double-layer model, they fail to reproduce the experimental[8] distances of 125 and 370 pm, perhaps again due to the neglecting of van der Waals interactions in the calculations. Furthermore, it might be that larger surface

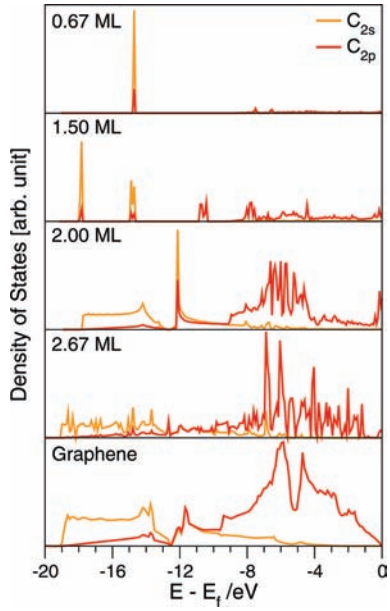

Figure 8. DOS plots of C(2s) and C(2p) states for the most stable arrangements of adsorbed carbon at different coverages on Pt(111). For comparison, also the DOS for graphene is shown.

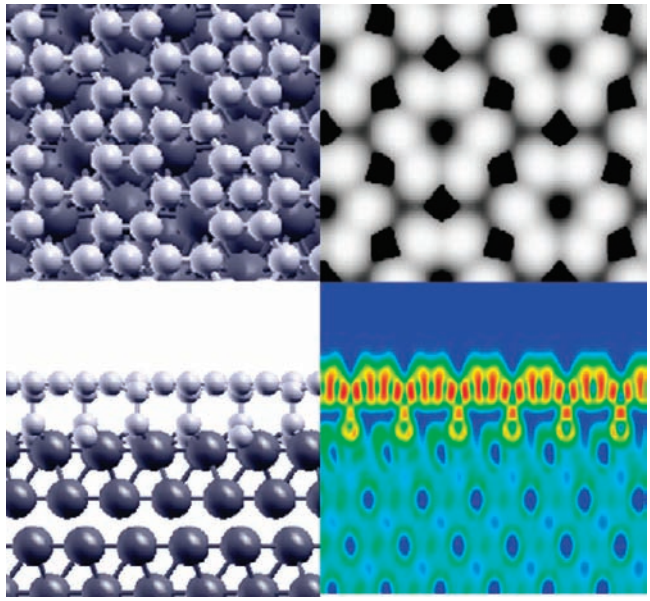

Figure 9. Calculated data for the double-layer model consisting of a carbidic phase and a graphene layer on Pt(111): (top left panel) the structural arrangement (top view); (bottom left panel) the structural arrangement (lateral view); (top right panel) constant-current STM image; (bottom right panel) ELF plot.

unit cells that take into account a possible lattice mismatch of graphene and Pt are required to reproduce the experimental layer distances. Finally, the DOS plots (Figure 10) show that both layers are different in nature; the topmost graphitic, showing an electronic structure typical to that of graphene, while the lowest presents a different electronic structure, especially with a more localized C(2s) band.

3.4. Evolution of Structures with the Coverage of C. This section gives an overview of the formation of carbon structures. Figure 11 shows the E_{ads} as well as the E^{int}_{PtC} and E^{int}_{CC} values for the most stable structures found in this study. Here, four different areas can be distinguished. The first one (I) is defined by low coverage $\theta_C = 0.30$ ML, when single C atoms adsorbed on *fcc* sites are the preferred arrangement. The interaction energies with

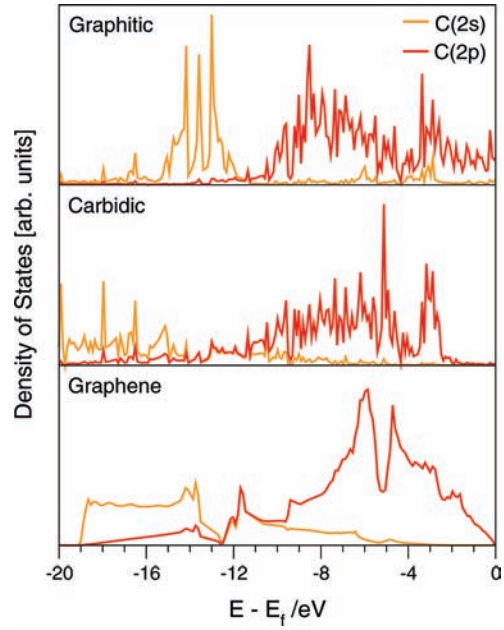

Figure 10. Comparison of the DOS of the carbidic layer (top) and graphitic layer (middle) of the double-layer model of graphene on Pt(111). For comparison, also the DOS of graphene is shown (bottom).

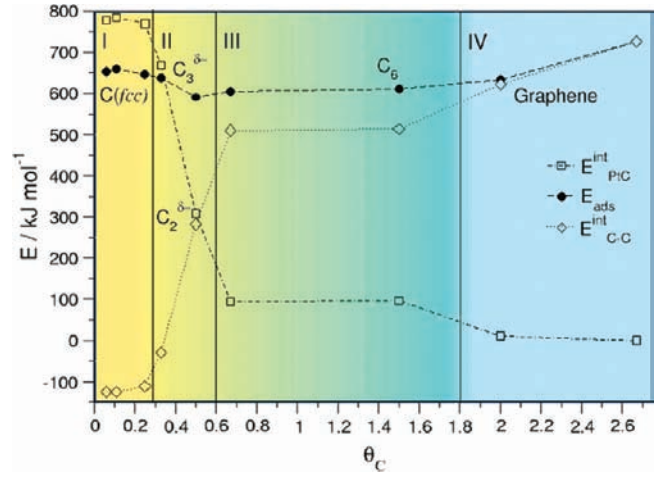

Figure 11. Evolution with carbon coverage (θ_C) of the adsorption energy per atom C, E_{ads} (black spots, dashed lines), the interaction energy of carbon with Pt(111), E^{int}_{PtC} (white squares, dashed−dotted lines), and the interaction energy between supported carbon atoms, E^{int}_{CC} (white diamonds, dotted lines). Roman numbers I−IV refer to carbidic, pseudocarbidic, pseudographitic, and graphitic zones, respectively.

the Pt surface are quite high (above 750 kJ mol^{-1}), and only partly counteracted by the Couloumb repulsions of negatively charged C adatoms (of more than 100 kJ mol^{-1}). Coverages between ~0.30 and ~0.60 ML define section II, where coverage becomes high enough, such that the repulsions are so intense that the formation of small aggregates of C atoms is feasible. Trimers of C atoms adsorbed on *fcc* sites around surface Pt atoms are stable at a coverage of 0.33 ML. Calculations of these trimers imply that surface Pt atoms are pulled above the adsorbed C atoms, accompanied by a loss of charge on Pt atoms (+0.12 e), which reduces the work function to 4.89 eV. However, the interactions with the substrate are still quite strong. The situation changes at a coverage of 0.50 ML, when dimers start to be formed through a covalent bond between carbon atoms. This situation yields the lowest adsorption energy and implies similar interaction strengths between carbon atoms and

with the surface. Coverages above ∼0.60 ML define section III, characterized by the formation of benzene-like rings, with high interaction energies between them and very weak interaction with the substrate (below 100 kJ mol^{-1}). At this point, the rings are expected to be mobile enough to gather on the Pt(111) surface. The weak interaction with the substrate essentially vanishes in section IV (defined by coverages above ∼1.8 ML), when graphene layers start to be formed.

4. Conclusions

We studied the formation of carbonaceous deposits on Pt(111) surfaces and Pt nanoparticles using suitable models and state-of-the-art DF calculations. The study ranges from the very first initial stages of carbon deposition to a final formation of graphene monolayers.

A carbidic phase is formed below a coverage of ∼0.3 ML, when negatively charged carbon adatoms adsorb strongly, preferentially over *fcc* hollow sites. A diffusion temperature about 475 ± 10 K for such adatoms is predicted on the basis of calculated energies. On Pt nanoparticles, the adsorption of C atoms seems to be enhanced near particle edges, especially for the *hcp* sites, partly due to the special flexibility of defect sites, which assists to accommodate the C adatoms.

Above a coverage of ∼0.3 ML, the mutual repulsion between isolated C adatoms is high enough, such that the formation of small aggregates becomes favorable. In fact, C_3 and C_2 species are predicted to form at coverages of 0.33 and 0.5 ML, respectively. The C_3 species are formed by C atoms adsorbed over *fcc* sites around a surface Pt atom, which unexpectedly is pulled outward from the surface while becoming positively charged. In fact, such a situation might imply a distinct reactivity of such above-the-plane Pt atoms. The calculations suggest that an identification of the C_3 species might be possible through a reduction of the work function to 4.89 eV at a coverage of 0.33 ML or through STM images.

C_2 species on Pt(111) exhibit a covalent bond, and the interaction strengths with the substrate and between the C atoms are comparable. Such reduction of the adhesion to the surface would suggest a strong mobility, and the C_2 dimers could be thought of as the key for the formation of benzene-like rings at coverages above 0.6 ML. These rings can be the building block of monolayer graphene. However, they remain to be isolated species up to a coverage of ∼1.8 ML, when the arrangement starts to exhibit the typical electronic structure of graphene.

A carbon double-layer model suggested experimentally has been studied and corroborated to be stable. A layer of carbidic C atoms is adsorbed on Pt(111), while a graphene layer is adsorbed on top of it. Some of the carbidic atoms serve as anchors for the graphene layer, with noticeable interaction energies and covalent bonds formed. This double-layer model would imply a much higher adhesion of the graphene layer than the single-layer model.

Acknowledgment. F.V. thanks the Alexander von Humboldt Foundation for financing his postdoctoral grant. K.M.N. is grateful to the Spanish Ministry MICINN for financial support via the grants FIS2008-02238, HA2006-0102, and CTQ2007-30547-E/BQU. The authors gratefully acknowledge the funding of the German Research Council (DFG) which, within the framework of its "Excellence Initiative", supports the Cluster of Excellence "Engineering of Advanced Materials" (www.eam.uni-erlangen.de) at the University of Erlangen-Nuremberg. We greatly acknowledge stimulating discussion with Prof. J. Libuda and Dr. Y. Lykhach.

References and Notes

(1) Davis, S. M.; Somorjai, G. A. In *The Chemical Physics of Solid Surfaces and Heterogeneous Catalysis*; King, D. A., Woodruff, D. P., Eds.; Elsevier: Amsterdam, The Netherlands, 1983; Vol. 4.
(2) Horsley, J. A. In *Chemistry and Physics of Solid Surfaces*; Vanselow, R., Howe, R., Eds.; Springer: Berlin, 1990.
(3) Borodziński, A.; Bond, G. C. *Catal. Rev.—Sci. Eng.* **2006**, *48*, 91.
(4) Zhang, Z. L.; Verykios, X. E. *Catal. Today* **1994**, *21*, 589.
(5) Baron, K.; Blakely, D. W.; Somorjai, G. A. *Surf. Sci.* **1974**, *41*, 45.
(6) Hamilton, J. C.; Blakely, D. W. *Surf. Sci.* **1980**, *90*, 199.
(7) Lang, B. *Surf. Sci.* **1975**, *53*, 317.
(8) Zi-pu, H.; Ogeltree, D. F.; van Hove, M. A.; Somorjai, G. A. *Surf. Sci.* **1987**, *180*, 433.
(9) Idakiev, V.; Tabakova, T.; Yuan, Z. Y.; Su, B. L. *Appl. Catal., A* **2004**, *270*, 135.
(10) Wang, X.; Rodríguez, J. A.; Hanson, J. C.; Gamarra, D.; Martinez-Arias, A.; Fernandez-Garcia, M. *J. Phys. Chem. B* **2005**, *109*, 19595.
(11) Sakurai, H.; Akita, T.; Tsubota, S.; Kiuchi, M.; Haruta, M. *Appl. Catal., A* **2005**, *291*, 197.
(12) Wang, X.; Rodríguez, J. A.; Hanson, J. C.; Perez, M.; Evans, J. *J. Chem. Phys.* **2005**, *123*, 221101.
(13) Bitter, J. H.; Seshan, K.; Lercher, J. A. *J. Catal.* **1999**, *183*, 336.
(14) Psofogiannakis, G.; St-Amant, A.; Ternan, M. *J. Phys. Chem. B* **2006**, *110*, 24593.
(15) Land, T. A.; Michely, T.; Behm, R. J.; Hemminger, J. C.; Comsa, G. *J. Chem. Phys.* **1992**, *97*, 6774.
(16) Land, T. A.; Michely, T.; Behm, R. J.; Hemminger, J. C.; Comsa, G. *Surf. Sci.* **1992**, *264*, 261.
(17) Vincent, R. S.; Lindstedt, R. P.; Malik, N. A.; Reid, I. A. B.; Messenger, B. E. *J. Catal.* **2008**, *260*, 37.
(18) Fujita, T.; Kobayashi, W.; Oshima, C. *Surf. Interface Anal.* **2005**, *37*, 120.
(19) Nakao, K.; Watanabe, O.; Sasaki, T.; Ito, S.; Tomishige, K.; Kunimori, K. *Surf. Sci.* **2007**, *601*, 3796.
(20) McCrea, K. R.; Parker, J. S.; Somorjai, G. A. *J. Phys. Chem. B* **2002**, *106*, 10854.
(21) Su, X.; Cremer, P. S.; Shen, Y. R.; Somorjai, G. A. *J. Am. Chem. Soc.* **1997**, *119*, 3994.
(22) Bowker, M.; Jones, I. Z.; Bennett, R. A.; Esch, F.; Baraldi, A.; Lizzit, S.; Comelli, G. *Catal. Lett.* **1998**, *51*, 187.
(23) Cambell, C. T.; Ertl, G.; Kuipers, H.; Segner, J. *J. Chem. Phys.* **1990**, *73*, 5862.
(24) Langmuir, I. *Trans. Faraday Soc.* **1922**, *17*, 672.
(25) Berlowitz, P. J.; Peden, C. H. F.; Goodman, D. W. *J. Phys. Chem.* **1988**, *92*, 5213.
(26) Uetsuka, H.; Watanabe, K.; Kimpara, H.; Kunimori, K. *Langmuir* **1999**, *15*, 5795.
(27) Nakao, K.; Ito, S.; Tomishige, K.; Kunimori, K. *Chem. Phys. Lett.* **2005**, *410*, 17553.
(28) Engel, T.; Ertl, G. *Adv. Catal.* **1979**, *28*, 1.
(29) Starr, D. E.; Pazhetnov, E. M.; Stadnichenko, A. I.; Boronin, A. I.; Shaikhutdinov, S. K. *Surf. Sci.* **2006**, *600*, 2688.
(30) Shelton, J. C.; Patil, H. R.; Blakeley, J. M. *Surf. Sci.* **1974**, *43*, 493.
(31) Ueta, H.; Saida, M.; Nakai, C.; Yamada, Y.; Sasaki, M.; Yamamoto, S. *Surf. Sci.* **2004**, *560*, 183.
(32) Aizawa, T.; Souda, R.; Otani, S.; Ishizawa, Y.; Oshima, C. *Phys. Rev. Lett.* **1990**, *64*, 768.
(33) Aizawa, T.; Hwang, Y.; Hayami, W.; Souda, R.; Otani, S.; Ishizawa, Y. *Surf. Sci.* **1992**, *260*, 311.
(34) Nagashima, A.; Tejima, N.; Oshima, C. *Phys. Rev. B* **1994**, *50*, 17487.
(35) Wu, X.-L.; Zhou, P.; Lieber, C. M. *Phys. Rev. Lett.* **1988**, *61*, 2604.
(36) Itoh, H.; Ichinose, T.; Ichinokawa, T. *Surf. Sci.* **1991**, *254*, L437.
(37) Echanescu, M.; Schleef, D.; Ogletree, D. F.; Salmeron, M. *Phys. Rev. B* **1999**, *60*, 16913.
(38) Sasaki, M.; Yamada, Y.; Ogiwara, Y.; Yagyu, S.; Yamamoto, S. *Phys. Rev. B* **2000**, *61*, 15653.
(39) Johánek, V.; De La Ree, A. B.; Hemminger, J. C. *J. Phys. Chem. C* **2009**, *113*, 4441.
(40) Yamada, Y.; Sinsarp, A.; Sasaki, M.; Yamamoto, S. *Jpn. J. Appl. Phys.* **2002**, *41*, 7501.
(41) Giunta, P. L.; Kelty, S. P. *J. Chem. Phys.* **2001**, *114*, 1807.
(42) Oshima, C.; Nagashima, A. *J. Phys.: Condens. Matter* **1997**, *9*, 1.
(43) Ishizawa, Y.; Koizumi, M.; Oshima, C.; Otani, S. *J. Phys. Coll.* **1987**, *48*, C9.
(44) Koma, A. *Surf. Sci.* **1992**, *267*, 29.
(45) Creighton, J. R.; White, J. M. *Surf. Sci.* **1983**, *129*, 327.
(46) Pettiette-Hall, C. L.; Land, D. P.; McIver, R. T.; Hemminger, J. C. *J. Phys. Chem.* **1990**, *94*, 1948.

(47) Hutson, F. L.; Ramaker, D. E.; Koel, B. E. *Surf. Sci.* **1991**, *248*, 104.
(48) Zhou, X.-L.; Zhu, X.-Y.; White, J. M. *Surf. Sci.* **1988**, *193*, 387.
(49) Pazhetnov, E. M.; Koshcheev, S. V.; Boronin, A. I. *Kinet. Katal. Engl. Transl.* **2003**, *44*, 1.
(50) Wang, S.-G.; Liao, X.-Y.; Cao, D.-B.; Li, Y.-W.; Wang, J.; Jiao, H. *J. Phys. Chem. C* **2007**, *111*, 10894.
(51) Levy, R. B.; Boudart, M. *Science* **1973**, *181*, 547.
(52) Viñes, F.; Rodriguez, J. A.; Liu, P.; Illas, F. *J. Catal.* **2008**, *260*, 103.
(53) Viñes, F.; Sousa, C.; Liu, P.; Rodriguez, J. A.; Illas, F. *J. Chem. Phys.* **2005**, *122*, 174709.
(54) Rosei, R.; De Crescenzi, M.; Sitte, F.; Quaresima, C.; Savoia, A.; Perfetti, P. *Phys. Rev. B* **1983**, *28*, 1161.
(55) Okamoto, Y. *Chem. Phys. Lett.* **2005**, *407*, 354.
(56) Park, S.-II.; Quate, C. F. *Appl. Phys. Lett.* **1986**, *48*, 112.
(57) Kuwabara, M.; Clarke, D. R.; Smith, D. A. *Appl. Phys. Lett.* **1990**, *56*, 2396.
(58) Binnig, G.; Fuchs, H.; Gerber, Ch.; Rohrer, H.; Stoll, E.; Tosatti, E. *Europhys. Lett.* **1986**, *1*, 31.
(59) Tersoff, J. *Phys. Rev. Lett.* **1986**, *57*, 440.
(60) Selloni, A.; Carnevali, P.; Tosatti, E.; Chen, C. D. *Phys. Rev. B* **1985**, *31*, 2602.
(61) Batra, I. P.; Garcia, N.; Rohrer, H.; Salemink, H.; Stoll, E.; Ciraci, S. *Surf. Sci.* **1987**, *181*, 126.
(62) Soler, J. M.; Baro, A. M.; Garcia, N.; Roher, H. *Phys. Rev. Lett.* **1986**, *57*, 444.
(63) Kresse, G.; Furthmüller, J. *Phys. Rev. B* **1996**, *54*, 11169.
(64) Blöchl, P. E. *Phys. Rev. B* **1994**, *50*, 17953.
(65) Görling, A.; Trickey, S. B.; Gisdakis, P.; Rösch, N. In *Topics in Organometallic Chemistry*; Brown, J., Hofmann, P., Eds.; Springer: Heidelberg, Germany, 1999; Vol. 4, p 109.
(66) Roldán, A.; Viñes, F.; Illas, F.; Ricart, J. M.; Neyman, K. M. *Theor. Chem. Acc.* **2008**, *120*, 565.
(67) Vosko, S. H.; Wilk, L.; Nusair, M. *Can. J. Phys.* **1980**, *58*, 1200.
(68) Perdew, J. P.; Wang, Y. *Phys. Rev. B* **1992**, *45*, 13244.
(69) Perdew, J. P.; Burke, K.; Ernzerhof, M. *Phys. Rev. Lett.* **1996**, *77*, 3865.
(70) Hammer, B.; Hansen, L. B.; Nørskov, J. K. *Phys. Rev. B* **1999**, *59*, 7413.
(71) Kittel, C. *Introduction to Solid State Theory*, 6th ed.; Wiley: New York, 1986; pp 55−57.
(72) Kittel, C. *Introduction to Solid State Theory*, 5th ed.; Wiley: New York, 1976; p 74.
(73) Yudanov, I. V.; Sahnoun, R.; Neyman, K. M.; Rösch, N. *J. Chem. Phys.* **2002**, *117*, 9887.
(74) Viñes, F.; Illas, F.; Neyman, K. M. *Angew. Chem., Int. Ed.* **2007**, *46*, 7094.
(75) Viñes, F.; Illas, F.; Neyman, K. M. *J. Phys. Chem. A* **2008**, *112*, 8911.
(76) Viñes, F.; Desikusumastuti, A.; Staudt, T.; Görling, A.; Libuda, J.; Neyman, K. M. *J. Phys. Chem. C* **2008**, *112*, 16539.
(77) Viñes, F.; Loschen, C.; Illas, F.; Neyman, K. M. *J. Catal.* **2009**, *226*, 59.
(78) Parades-Olivera, P.; Patrito, E. M.; Sellers, H. L. *Surf. Sci.* **1995**, *327*, 330.
(79) Kuz'min, I. V.; Zeigarnik, A. V. *Kinet. Catal.* **2004**, *45*, 561.
(80) Michaelides, A.; Hu, P. *J. Chem. Phys.* **2001**, *114*, 5792.
(81) Kua, J.; Goddard III, A. *J. Phys. Chem. B* **1998**, *102*, 9492.
(82) Zhu, X. Y.; Huang, X. J. *Physica B* **2007**, *400*, 287.
(83) This estimation implies a first-order kinetics of the Redhead equation. For the present estimations, an α value of 10^8 s^{-1} was employed.
(84) Brandt, B.; Fischer, J.-H.; Ludwig, W.; Libuda, J.; Zaera, F.; Schauermann, S.; Freund, H.-J. *J. Phys. Chem. C* **2008**, *112*, 11408.
(85) Teschner, D.; Révay, Z.; Borsodi, J.; Hävecker, M.; Knop-Gericke, A.; Schlögl, R.; Milroy, D.; Jackson, S. D.; Torres, D.; Sautet, P. *Angew. Chem., Int. Ed.* **2008**, *47*, 9274.
(86) Wilde, M.; Fukutani, K.; Ludwig, W.; Brandt, B.; Fischer, J.-H.; Schauermann, S.; Freund, H.-J. *Angew. Chem., Int. Ed.* **2008**, *47*, 9289.
(87) Teschner, D.; Borsodi, J.; Wootsch, A.; Révay, Z.; Hävecker, M.; Knop-Gericke, A.; Jackson, S. D.; Schlögl, R. *Science* **2008**, *320*, 86.
(88) Gracia, L.; Calatayud, M.; Andrés, J.; Minot, C.; Salmeron, M. *Phys. Rev. B* **2005**, *71*, 033407.
(89) Yudanov, I. V.; Neyman, K. M.; Rösch, N. *Phys. Chem. Chem. Phys.* **2004**, *6*, 116.
(90) Lim, K. H.; Neyman, K. M.; Rösch, N. *Chem. Phys. Lett.* **2006**, *432*, 184.
(91) Studt, F.; Abild-Pedersen, F.; Bligaard, T.; Sørensen, R. Z.; Christensen, C. H.; Nørskov, J. K. *Angew. Chem., Int. Ed.* **2008**, *47*, 9299.
(92) Shiraishi, M.; Ata, M. *Carbon* **2001**, *39*, 1913.

JP903653Z